European Journal of Material Science

Vol.8, No.1, pp.1-12, 2021

Print ISSN: ISSN 2055-6551(Print), Online ISSN: ISSN 2055-656X (Online)

DEPENDENCE OF OPTICAL BAND GAP ON CRYSTALLITE SIZE OF TIO_2 THIN FILMS PREPARED USING SOL GEL PROCESS

Benjamin Mbaluka John[1, 2], Simon W. Mugo[1] and James M. Ngaruiya[1]

[1](Department of Physics, Jomo Kenyatta University of Agriculture and Technology (JKUAT), Nairobi Kenya)

[2](Department of Physics and Electronics, South Eastern Kenya University (SEKU), Kitui Kenya)

ABSTRACT: *We report on a simple and robust analysis of the energy band gap and crystal size of anatase TiO_2 thin films on doped Fluorine Tin Oxide (SnO_2:F) prepared using sol-gel Doctor-blade method. The films had been annealed at rates of 1°C/Min, 2°C/Min, 1-step and referenced with as-deposited film, and the optical and structural properties characterized using UV-VIS spectrophotometer and X-ray diffraction (XRD), respectively. The films had a refractive index which was noted to depend on the annealing rate consistent with Cauchy's relation. An optical band gap of* $3.88eV$, $3.72eV$, $3.33eV$, *and* $3.13eV$ *was measured on the as-deposited, 1-Step, 2°C/Min and 1°C/Min annealing, respectively. Optical conductivity was highest in the UV region and diminished sharply in the visible region in all the annealed samples. The as-deposited film exhibited a diminished optical conductivity in the visible electromagnetic field due to high density of charge trapping sites resulting to negligible interaction of the film molecules with the applied electric field. The XRD spectra revealed thermal enhancement in crystallinity, with the crystallite sizes of* $21.8382nm$, $24.3087nm$ *and* $24.9633nm$, *for 1-step annealed, 2°C/Min and 1°C/Min, respectively. The broadened XRD spectrum of the as-deposited film is attributed to the presence of dangling bonds that act as trapping sites. Comparison of the measured values of the optical band gap with simulation from SCOUT at low annealing rates (2°C/min and 1°C/min) was found to decrease with enhancement in crystallite size, indicating a reduction in porosity and improvement in both densification and crystallinity of the films.*

KEYWORDS: *TiO_2, band gap, refractive index, crystal size, photon energy,*

INTRODUCTION

Titanium dioxide (TiO_2) has received remarkable attention due to its unique optical, photocatalytic, structural and electronic properties [1-2]. The wide band gap, high refractive index, and good chemical stability, makes TiO_2 thin films find a wide application in optical coatings [3-4], dye-sensitized solar cells (DSSCs) [5] and in dielectrics [6]. Additionally, the high transparency of the films makes them a candidate for anti-reflection coatings as they enhance the visible transmittance in heat mirrors [7]. On structure, TiO_2 thin films can exist as amorphous as well as in other three crystalline phases, namely rutile (tetragonal), anatase (tetragonal and brookite (orthorhombic). Only the rutile phase is thermodynamically stable at high temperature [12]. Ye *et al.,* [8] reported refractive indices of 2.5 and 2.7 for bulk rutile and anatase titania, respectively, at $500nm$. Band gap values of $3.23eV$, $3.02eV$ and $3.13eV$ has been reported for Anatase, Rutile and

Brookite films, respectively [9]. However, these measurements for both band gaps and refractive indices have been found to vary with the structure of the films [11]. And since structural characterization requires specialized techniques, correlation of optical parameters with structure of TiO_2 films would offer an alternative that is more accessible to many. This work offers a simple, facile and robust method of correlating crystallite size with optical band gap of TiO_2 thin films prepared using Doctor-blade method.

Experimental Technique

Nanocrystalline TiO_2 films were prepared by doctor-blading titanium nanoxide T/SP (18% wt, Solaronix, Switzerland) on cleaned doped Fluorine Tin Oxide (FTO) (SnO_2:F) glass substrates. The drying process was done for 20 minutes in ambient temperature, to enhance homogeneity of the films. The films were then subjected to different annealing rates (1^oC/Min, 2^oC/Min) up to 450^oC and 1-step annealing in which the films were directly annealed at 450^oC) and then sintered at 450^oC for 30 minutes: A UV-VIS spectrometer (*Perkin Elmer Lambda 950),* was used to obtain the transmittance of the films within $250-800nm$ spectral wavelength. The measurements were obtained at a normal incidence using a reference substrate. For structure, the film crystalline phases were characterized using X-ray diffractometer (*K alpha 1504Armstrongs*) with a Cu - K_α radiation ($K_\alpha = 0.15406nm$) and operating at an accelerating voltage of 40kV and an emission current of $40\,mA$. Data was acquired over a range of ($20^o \le 2\theta \le 80^o$) grazing angle at a sampling width of 0.1^o and a scanning speed of $1.2^o\,\text{min}^{-1}$.

RESULTS AND DISCUSSION

Part 1: Optical measurements

(a) Refractive Index

The refractive indices were obtained from the transmittance spectra based on the Swanepoel method [10]. The refractive index (n_f) in the spectral region of medium and weak absorption was calculated based on equations 1 and 2.

$$n_f = \sqrt{N + \sqrt{N^2 - n_s^2}} \quad \text{.....(1)}$$

$$n_s = \frac{1}{T_s} + \left(\frac{1}{T_s} - 1\right)^{1/2} \quad \text{.....(2)}$$

Where $N = 2n_s \dfrac{T_M - T_m}{T_M T_m} + \dfrac{n_s^2 + 1}{2}$, T_M and T_m are the maximum and minimum transmissions corresponding to a certain wavelength λ. n_s and T_s are the refractive index and transmittance of the substrate, respectively. A plot of the refractive index against wavelength, shown in fig. 1, reveals that the refractive index of the films is high in the UV region (region of strong absorption) and reduces with increasing wavelength (region of weak and medium absorption). This trend is noted to be consistent with Cauchy's-Model [24]. The *as*-deposited films had the lowest refractive

index of 2.325 which improved upon annealing. Films annealed at 1°C/Min has the highest refractive index of 2.55 at $550nm$.

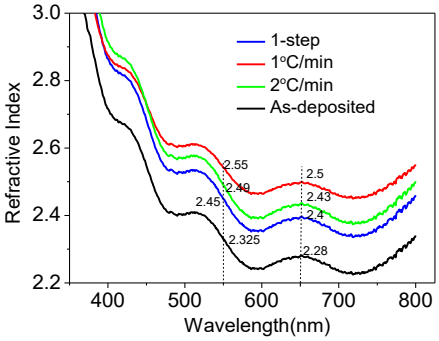

Figure 1: Plot of Refractive Index against wavelength

The enhancement in refractive index at low annealing rates is attributed to the increase in packing density of the films [17]. The high annealing rate results to reduced porosity which consequently leads to densification of the films [21, 25].

(b) Porosity

The porosity (P) of the TiO_2 films was determined using eqn. 3, [13, 34, 35].

$$P(\%) = \left(1 - \frac{n^2 - 1}{n_b^2 - 1}\right) \times 100 \text{.....(3)}$$

Where n is the refractive index of the porous thin films and $n_b=2.52$ is the refractive index of pore-free anatase film obtained at $550nm$ [13,11].

A correlation of porosity and refractive index versus annealing rates (Fig. 2), shows an inverse relation.

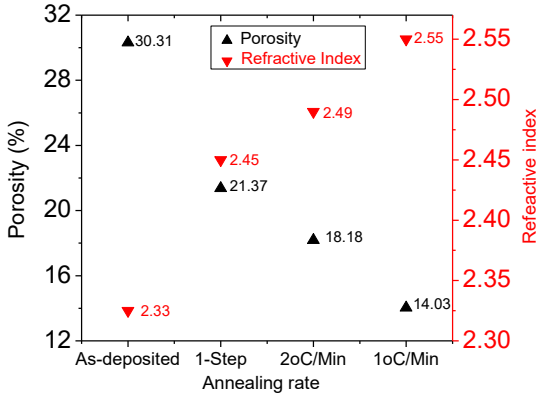

Figure 2: Correlation between porosity and refractive index versus annealing rate

Films annealed at 1°C/Min exhibit a low porosity (14.03%) and a high refractive index (2.55). On the contrary, the *as*-deposited films exhibit a high porosity (30.31%) and lowest refractive index (2.33). This is attributed to the fact that at low annealing rates, the pore size reduced due to grain's compaction and densification. Hence, the TiO_2 film becomes more densely packed leading to high refractive index and reduced porosity [36, 37].

(c) Optical Band Gap

The optical band gap (E_g) was calculated using the Tauc equation, eqn. 4, [14].

$$(\alpha h\upsilon)^r = A(h\upsilon - E_g) \quad \text{.....(4)}$$

Where α is the absorption coefficient given by:

$$\alpha = \left(\frac{1}{d}\right)\ln\left(\frac{1}{T}\right) \quad \text{.....(5)},$$

$h\upsilon$ is the photon energy, r is the transition coefficient ($r = 2$ and $r = 1/2$ for direct and indirect transitions, respectively), d is film thickness and A is a parameter of transition probability given by eqn. 6, [34].

$$A = \frac{4\pi\sigma_{\min}}{nc\Delta E} \quad \text{.....(6)}$$

$\sigma_{\min}$ is the minimum metallic conductivity, c speed of light and $\Delta E = \Delta E_c - \Delta E_V$ represents band tailing. The transition coefficient r depends on the material's structure [34]. Since indirect transition dominates in nanostructured TiO_2, we have adopted $r = 1/2$ [17]. The optical band gap was determined from the extrapolation of the linear plots of $(\alpha h\upsilon)^{1/2}$ versus $h\upsilon$ at $\alpha = 0$, as shown in figure 3. The band gap was found to decrease with decrease in annealing rate, 3.88, 3.72, 3.33, and 3.13eV for the *as*-deposited, 1-step, 2°C/Min and 1°C/Min annealed films, respectively.

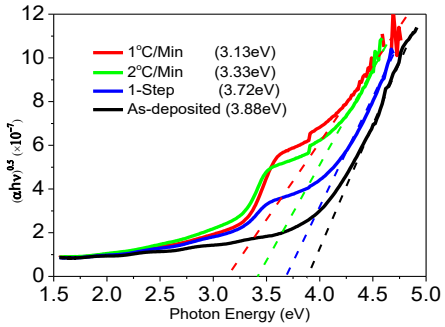

Figure 3: Optical energy band gap for TiO_2 films as a function of photon energy

The decrease in optical band gap with the decrease in annealing rate is attributed to the lowering of interatomic spacing, which is associated with a decrease in the amplitude of atomic oscillations around their equilibrium positions [17, 16, 21]. This points to better crystallization as small crystallites agglomerate into large crystals [20, 22, 29]. Low annealing rate enhances the formation of oxygen vacancies, and as a result the electron concentration increases in the energy gap region. This leads to some of the localized electronic states approaching the conduction band to be at minimum. Thus, at lower annealing rate, anatase TiO_2 behaves as *n*-type semiconductor due to reduced optical band gap [30, 31].

To complement the experimental data, we also simulated the optical energy band gap using SCOUT's OJL model. A near correlation was arrived at, with only a deviation of $0.12eV$ and $0.03eV$ recorded for the 1°C/Min and 2°C/Min annealing, respectively (fig. 4).

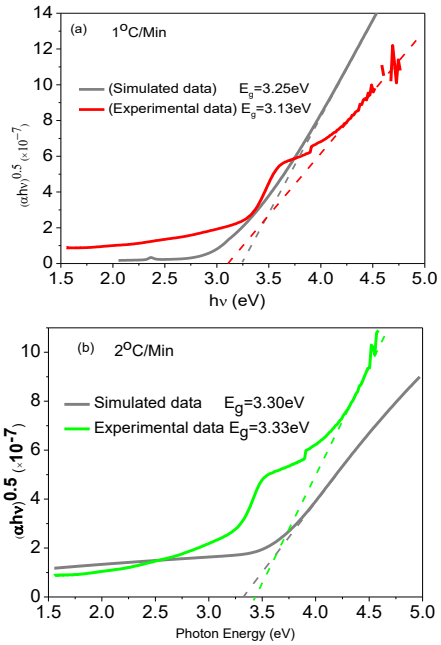

Figure 4: Comparison of the measured and OJL model simulated data for: 4(a) 1°C/Min and 4(b) 2°C/Min TiO_2 thin films.

The experimental band gap shows a good approximation to the theoretical values.

(d) Dielectric Constant

The real (ε_r) and imaginary dielectric constants (ε_i) for the films were calculated based on the complex refractive index as shown in equations 7 [23].

$$\varepsilon = \varepsilon_r - i\varepsilon_i : \ \varepsilon_r = n^2 - k^2, \ \varepsilon_i = 2nk \text{.....(7)}$$

Where k is the extinction coefficient. The ε_r and ε_i indicate the extent to which TiO_2 films slow down the speed of incident light and the extent to which dielectric absorbs energy from the applied

electric field due to dipole motion, respectively [19, 23]. The ratio of ε_i to ε_r is the Loss tangent ($\tan\delta$) and is a measure of the extent to which thin films absorb the electromagnetic (EM) field [30] (Eqn. 8).

$$Tan\delta = \frac{\varepsilon_i}{\varepsilon_r} = \frac{2nk}{n^2 - k} = ...(8)$$

Where δ is the phase different between the induced current and the applied EM field [34]. A plot of $\tan\delta$ versus wavelength is shown in fig. 5.

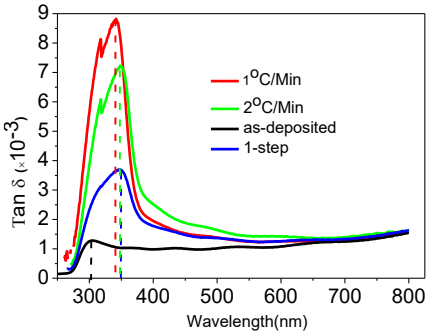

Figure 5: Variation of Loss Tangent ($\tan\delta$) with wavelength.

ε_i decreases faster than the ε_r in the UV region as indicated by high $\tan\delta$ and diminishes sharply at the onset of the visible region. This indicates reduced absorption in the visible regime. The films annealed at 1°C/Min have the highest $\tan\delta$ in the UV region, an indication of the highest changes in the free carrier's transitions in certain energy band that causes absorption [35]. Hence, $\tan\delta$ is enhanced resulting to high absorption of EM field [35].

(e) Optical Conductivity

Optical conductivity (σ) was determined using equation (9), [23, 30].

$$\sigma = \sigma_r + i\sigma_{im} = \frac{\alpha nc}{4\pi} .....(9)$$

Where $\sigma_r = \omega\varepsilon_o\varepsilon_{im}$, $\sigma_{im} = \omega\varepsilon_0\varepsilon_r$, $\varepsilon = \varepsilon_r - i\varepsilon_{im}$, ω is the angular frequency, ε_o is the free space dielectric constant and c is the velocity of light [15, 16, 35].

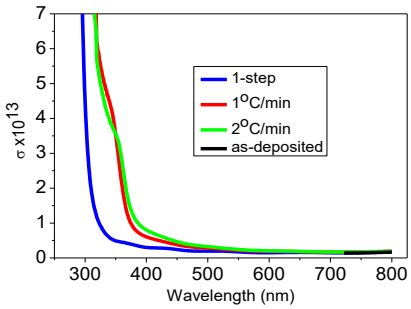

Figure 6: Optical conductivity spectra versus wavelength.

Figure 6 shows that the optical conductivity is high in the UV spectral region and decreases drastically in the visible region for the annealed films. The phenomenon implies that electrons are excited by the high photon energy in the UV region. Further, the films annealed at 1°C/Min and 2°C/Min exhibit a wider spectral range ($250-375nm$) of electron excitation as compared with the 1-step annealed film ($250-325nm$), a behavior attributed to drastic reduction in energy band gap. It is also observed that the *as*-deposited film only exhibit optical response in the $712.5-800nm$ spectral range due to the lack of delocalized carriers in its large band gap as well as its disordered state [35, 38]. The optical conductivity decreased corresponding to the absorption edge and energy band gap of the films [35].

Part 2: Structural measurement

(a) X-ray diffraction measurements

The phase composition and the structure of the films were studied by X-ray diffraction analysis. From the data, Bragg's equation was used to determine planner $d-$spacing between atoms in the TiO_2 films. The diffraction peak observed in each diffraction pattern was also used to calculate the Miller indices and lattice spacing of the samples. The preferred orientations were determined using *Crystalism* software [27, 28] and the data plotted as shown in figure 7.

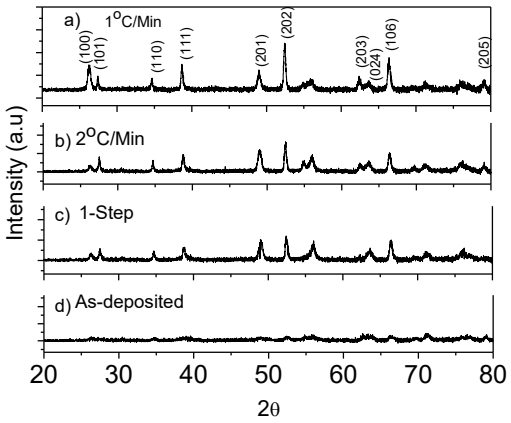

Figure 7: X-ray diffraction pattern of the TiO_2 films.

The observed peaks in Fig. 7(a) correspond to (100), (101), (110), (111), (201), (202), (203), (024), (106) and (205) planes for various 2θ angles and depict the formation of well crystallized TiO_2

thin films indicated by sharp diffraction peaks [26]. The diffraction pattern observed in the annealed films in Fig. 7(a), (b) and (c) indicates diffraction peaks at various glancing angles by planes of the anatase crystalline phase of TiO_2 annealed at different rates. In contrast, Fig. 7(d), exhibit rudimentary broad diffraction peaks corresponding to the as-deposited film. This is due to the film's amorphous nature [30]. The average nanocrystalline size (D) was calculated using Scherrer formula (Eqn. 10) [32].

$$D = \frac{K\lambda}{\beta \cos\theta} \text{.....(10)}$$

Where D (in nm) is mean size of the crystalline domains in the direction normal to the reflecting planes, β (in radians) is the Full-Width at Half Maximum (FWHM) of the peak, $K = 0.90$ is Scherrer constant, λ is X-ray wavelength, and θ (in radians) is the Bragg angle [13,17]. The FWHM of the XRD scans of TiO_2 films was obtained using *OriginPro 8.0* software and used to calculate the crystallite size according to eqn. 10. The average crystallite size was estimated at $24.9633, 24.3087$, and $21.8382nm$ for 1^oC/Min, 2^oC/Min and 1-step annealed films, respectively. The large crystallite size observed in 1^oC/Min annealed film was attributed to the gradual agglomeration of small crystallites into large ones [11, 33]. The *as*-deposited film is characterized by short-range order and contain many defects that produce localized states [33]. Therefore, by lowering the annealing rate, the defects are annealed out, hence the film crystallinity is improved and the crystallite size increases [30, 34].

(b) Correlation of Band gap with Crystal Size

The band gap and crystal size data was tabulated as shown in table 1. The as-deposited film indicates amorphous nature while the annealed films indicate some level of crystallinity.

Table 1. A table of Optical Band Gap and Crystal Size of the TiO_2 films annealed at different rates.

Annealing Rate	Band Gap (eV) (Experimental)	Band Gap (eV) (Simulated)	Crystal Size (*nm*)
1^oC/Min	3.13	3.25	24.96
2^oC/Min	3.33	3.30	24.31
1-step	3.72	3.25	21.84
As-deposited	3.88	3.63	

The variation in optical energy band gap and crystal size depends on the annealing rate (Fig. 8 and have a significant bearing on the band structure of TiO_2 thin films [25].

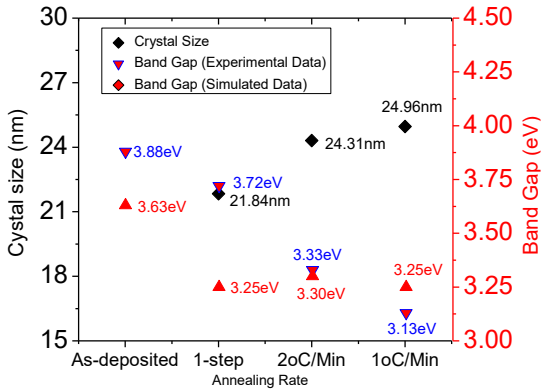

Figure 8: Variation of Optical Band Gap (from measurements and OJL's simulation) and Crystal Size versus Annealing Rate.

From figure 8, the crystal size increases with increase in annealing rate (21.84, 24.3, and 24.96*nm* for the 1-step, 2°C/Min and 1°C/Min, respectively). On the other hand, the Optical band gap decreases with decrease in Annealing rate (3.88, 3.72, 3.33 and 3.13eV for the as-deposited, 1-step, 2°C/Min and 1°C/Min, respectively). The experimental data for band gap coincides well with the simulated data, an indication of a good approximation. The variations in both crystal size and optical band gap with annealing rate are attributed to densification which results in decrease in porosity [17, 18, 30]. For example, at 1°C/Min, the pore size diminished by grain's compaction. The film became more densely packed and, consequently, the refractive index increased and optical band gap decreased [29]. This leads to a large surface area for the films, which, consequently, enhances photocatalytic property of TiO_2 thin films [30].

Conclusion

The dependence of crystallite size on optical band gap in TiO_2 films annealed at different rates was investigated. The refractive index was consistent with Cauchy's relation. Low annealing rate (1°C/Min) resulted into the highest refractive index. Moreover, the porosity and optical band gap decrease with annealing rate. This was attributed to films' densification and improved crystallinity. The optical conductivity was high in the UV region for the annealed films due to electron excitation and decreased sharply in the visible region. The as-deposited film exhibited optical response only at low electric fields ($712.5-800nm$ spectral range) due to lack of delocalized carriers. Upon annealing, the structural investigation indicated improvement in the crystallite size from $21.8382nm$ to $24.3087nm$ for 1-step annealed and 1°C/Min, respectively. The as-deposited broadening of the XRD peaks indicated a disordered structure due to defects that are responsible for localized states.

References

1. Fujishima, A., & Honda, K. (1972). Electrochemical photolysis of water at a semiconductor electrode. *nature*, *238*(5358), 37.
2. Bak, T., Nowotny, J., Rekas, M., & Sorrell, C. C. (2002). Photo-electrochemical hydrogen generation from water using solar energy. Materials-related aspects. *International journal of hydrogen energy*, *27*(10), 991-1022.

3. Euvananont, C., Junin, C., Inpor, K., Limthongkul, P., & Thanachayanont, C. (2008). TiO2 optical coating layers for self-cleaning applications. *Ceramics International*, *34*(4), 1067-1071.
4. Kawasaki, H., Ohshima, T., Yagyu, Y., Suda, Y., Khartsev, S. I., & Grishin, A. M. (2008). TiO2/TiN/TiO2 heat mirrors by laser ablation of single TiN target. In *Journal of Physics: Conference Series* (Vol. 100, No. 1, p. 012038). IOP Publishing.
5. Sung, Y. M., & Kim, H. J. (2007). Sputter deposition and surface treatment of TiO2 films for dye-sensitized solar cells using reactive RF plasma. *Thin Solid Films*, *515*(12), 4996-4999.
6. Yang, W., & Wolden, C. A. (2006). Plasma-enhanced chemical vapor deposition of TiO2 thin films for dielectric applications. *Thin Solid Films*, *515*(4), 1708-1713.
7. Okada, M., Tazawa, M., Jin, P., Yamada, Y., & Yoshimura, K. (2006). Fabrication of photocatalytic heat-mirror with TiO2/TiN/TiO2 stacked layers. *Vacuum*, *80*(7), 732-735.
8. Ye, Q., Liu, P. Y., Tang, Z. F., & Zhai, L. (2007). Hydrophilic properties of nano-TiO2 thin films deposited by RF magnetron sputtering. *Vacuum*, *81*(5), 627-631.
9. Muaz, A. K. M., Hashim, U., Arshad, M. M., Ruslinda, A. R., Ayub, R. M., Gopinath, S. C., ... & Foo, K. L. (2016, July). Effect of annealing temperature on structural, morphological and electrical properties of nanoparticles TiO2 thin films by sol-gel method. In *AIP Conference Proceedings* (Vol. 1733, No. 1, p. 020087). AIP Publishing.
10. Swanepoel, R. (1983). Determination of the thickness and optical constants of amorphous silicon. *Journal of Physics E: Scientific Instruments*, *16*(12), 1214.
11. Hou, Y. Q., Zhuang, D. M., Zhang, G., Zhao, M., & Wu, M. S. (2003). Influence of annealing temperature on the properties of titanium oxide thin film. *Applied Surface Science*, *218*(1-4), 98-106.
12. Bakri, A. S., Sahdan, M. Z., Adriyanto, F., Raship, N. A., Said, N. D. M., Abdullah, S. A., & Rahim, M. S. (2017, January). Effect of annealing temperature of titanium dioxide thin films on structural and electrical properties. In *AIP conference proceedings* (Vol. 1788, No. 1, p. 030030). AIP Publishing.
13. Mathews, N. R., Morales, E. R., Cortés-Jacome, M. A., & Antonio, J. T. (2009). TiO2 thin films–Influence of annealing temperature on structural, optical and photocatalytic properties. *Solar Energy*, *83*(9), 1499-1508.
14. Zhao, B., Zhou, J., Chen, Y., & Peng, Y. (2011). Effect of annealing temperature on the structure and optical properties of sputtered TiO2 films. *Journal of Alloys and Compounds*, *509*(9), 4060-4064.
15. Sharma, P., & Katyal, S. C. (2007). Determination of optical parameters of a-(As2Se3) 90Ge10 thin film. *Journal of Physics D: Applied Physics*, *40*(7), 2115.
16. Pankove, J. I. (1975). *Optical processes in semiconductors*. Courier Corporation.
17. Sönmezoğlu, S., Çankaya, G., & Serin, N. (2012). Influence of annealing temperature on structural, morphological and optical properties of nanostructured TiO2 thin films. *Materials Technology*, *27*(3), 251-256.
18. Tian, G., Dong, L., Wei, C., Huang, J., He, H., & Shao, J. (2006). Investigation on microstructure and optical properties of titanium dioxide coatings annealed at various temperature. *Optical Materials*, *28*(8-9), 1058-1063.
19. Makhlouf, M. M., El-Denglawey, A., Zeyada, H. M., & El-Nahass, M. M. (2014). The structural and optical characterizations of tetraphenylporphyrin thin films. *Journal of Luminescence*, *147*, 202-208.

20. Salem, A. M., & Selim, M. S. (2001). Structure and optical properties of chemically deposited Sb2S3 thin films. *Journal of Physics D: Applied Physics*, *34*(1), 12.
21. Sunkara, B. K., & Misra, R. D. K. (2008). Enhanced antibactericidal function of W4+-doped titania-coated nickel ferrite composite nanoparticles: a biomaterial system. *Acta Biomaterialia*, *4*(2), 273-283.
22. Yarmand, B., & Sadrnezhaad, S. K. (2010). Influence of annealing temperature on structural and optical properties of mesoporous TiO2 thin films prepared by sol-gel templating technique. *Journal of Optoelectronics and Advanced Materials*, *12*(7), 1490.
23. Goswami A (2005): Thin Film Fundamental (New Delhi: New Age International) p 413
24. Ali, R., Saleem, M., Pääkkönen, P., & Honkanen, S. (2015). Thermo-optical properties of thin-film TiO2–Al2O3 bilayers fabricated by atomic layer deposition. *Nanomaterials*, *5*(2), 792-803.
25. Ravindra, N. M., Ganapathy, P., & Choi, J. (2007). Energy gap–refractive index relations in semiconductors–An overview. *Infrared physics & technology*, *50*(1), 21-29.
26. Govindasamy, G., Murugasen, P., & Sagadevan, S. (2016). Investigations on the synthesis, optical and electrical properties of TiO2 thin films by chemical bath deposition (CBD) method. *Materials Research*, *19*(2), 413-419.
27. Howard, C. J., Sabine, T. M., & Dickson, F. (1991). Structural and thermal parameters for rutile and anatase. *Acta Crystallographica Section B: Structural Science*, *47*(4), 462-468.
28. Ullah, Z., Atiq, S., & Naseem, S. (2013). Indexing the diffraction patterns and investigating the crystal structure of Pb-doped strontium ferrites. Journal of Scientific Research, 5(2), 235-244.
29. Bartic, M., Sacarescu, L., & Harabagiu, V. (2013). Optical and electrical properties of TiO2 thin films deposited by sol-gel method. *Revue Roumaine de Chimie*, *58*(2-3), 105-111.
30. El-Nahass, M. M., Soliman, H. S., & El-Denglawey, A. (2016). Absorption edge shift, optical conductivity, and energy loss function of nano thermal-evaporated N-type anatase TiO 2 films. *Applied Physics A*, *122*(8), 775.
31. Portillo-Vélez, N. S., Olvera-Neria, O., Hernández-Pérez, I., & Rubio-Ponce, A. (2013). Localized electronic states induced by oxygen vacancies on anatase TiO2 (101) surface. *Surface Science*, *616*, 115-119.
32. Deshmukh, H. P., Shinde, P. S., & Patil, P. S. (2006). Structural, optical and electrical characterization of spray-deposited TiO2 thin films. *Materials Science and Engineering: B*, *130*(1-3), 220-227.
33. Saini, K. K., Sharma, S. D., Kar, M., Singh, D., & Sharma, C. P. (2007). Structural and optical properties of TiO2 thin films derived by sol–gel dip coating process. *Journal of non-crystalline solids*, *353*(24-25), 2469-2473.
34. El-Nahass, M. M., Ali, M. H., & El-Denglawey, A. (2012). Structural and optical properties of nano-spin coated sol–gel porous TiO2 films. *Transactions of Nonferrous Metals Society of China*, *22*(12), 3003-3011.
35. El-Nahass, M. M., Soliman, H. S., & El-Denglawey, A. (2016). Absorption edge shift, optical conductivity, and energy loss function of nano thermal-evaporated N-type anatase TiO 2 films. *Applied Physics A*, *122*(8), 775.
36. Bartic, M., Sacarescu, L., & Harabagiu, V. (2013). Optical and electrical properties of TiO2 thin films deposited by sol-gel method. *Revue Roumaine de Chimie*, *58*(2-3), 105-111.

37. Ahn, Y. U., Kim, E. J., Kim, H. T., & Hahn, S. H. (2003). Variation of structural and optical properties of sol-gel TiO2 thin films with catalyst concentration and calcination temperature. *Materials Letters*, *57*(30), 4660-4666.
38. Nazarov, V. U. (1997). Surface dielectric response: Exact solution in the semiclassical infinite-barrier model with diffuse scattering. *Physical Review B*, *56*(4), 2198.